IJMMM International Journal of Minerals, Metallurgy and Materials 矿物冶金与材料学报（英文版）

Icosahedral quasicrystal structure of the $Mg_{40}Zn_{55}Nd_5$ phase and its thermodynamic stability

Shuai Zhang, Qianqian Li, Hongcan Chen, Qun Luo, and Qian Li

Cite this article as:
Shuai Zhang, Qianqian Li, Hongcan Chen, Qun Luo, and Qian Li, Icosahedral quasicrystal structure of the $Mg_{40}Zn_{55}Nd_5$ phase and its thermodynamic stability, *Int. J. Miner. Metall. Mater.*, 29(2022), No. 8, pp. 1543-1550. https://doi.org/10.1007/s12613-021-2391-2

View the article online at SpringerLink or IJMMM Webpage.

Articles you may be interested in

Wen-bo Luo, Zhi-yong Xue, and Wei-min Mao, Effect of heat treatment on the microstructure and micromechanical properties of the rapidly solidified $Mg_{61.7}Zn_{34}Gd_{4.3}$ alloy containing icosahedral phase, *Int. J. Miner. Metall. Mater.*, 26(2019), No. 7, pp. 869-877. https://doi.org/10.1007/s12613-019-1799-4

A. V. Koltygin, V. E. Bazhenov, R. S. Khasenova, A. A. Komissarov, A. I. Bazlov, and V. A. Bautin, Effects of small additions of Zn on the microstructure, mechanical properties and corrosion resistance of WE43B Mg alloys, *Int. J. Miner. Metall. Mater.*, 26(2019), No. 7, pp. 858-868. https://doi.org/10.1007/s12613-019-1801-1

Hong-xiang Li, Shi-kai Qin, Ying-zhong Ma, Jian Wang, Yun-jin Liu, and Ji-shan Zhang, Effects of Zn content on the microstructure and the mechanical and corrosion properties of as-cast low-alloyed Mg–Zn–Ca alloys, *Int. J. Miner. Metall. Mater.*, 25(2018), No. 7, pp. 800-809. https://doi.org/10.1007/s12613-018-1628-1

Gao-jie Li, Ming-xing Guo, Yu Wang, Cai-hui Zheng, Ji-shan Zhang, and Lin-zhong Zhuang, Effect of Ni addition on microstructure and mechanical properties of Al-Mg-Si-Cu-Zn alloys with a high Mg/Si ratio, *Int. J. Miner. Metall. Mater.*, 26(2019), No. 6, pp. 740-751. https://doi.org/10.1007/s12613-019-1778-9

Ying-zhong Ma, Chang-lin Yang, Yun-jin Liu, Fu-song Yuan, Shan-shan Liang, Hong-xiang Li, and Ji-shan Zhang, Microstructure, mechanical, and corrosion properties of extruded low-alloyed Mg–*x*Zn–0.2Ca alloys, *Int. J. Miner. Metall. Mater.*, 26(2019), No. 10, pp. 1274-1284. https://doi.org/10.1007/s12613-019-1860-3

Ping-chao Ke, Zhi-hong Liu, and Lin Li, Synthesis, characterization, and property test of crystalline polyferric sulfate adsorbent used in treatment of contaminated water with a high As(III) content, *Int. J. Miner. Metall. Mater.*, 25(2018), No. 10, pp. 1217-1225. https://doi.org/10.1007/s12613-018-1674-8

International Journal of Minerals, Metallurgy and Materials
Volume 29, Number 8, August 2022, Page 1543
https://doi.org/10.1007/s12613-021-2391-2

Icosahedral quasicrystal structure of the $Mg_{40}Zn_{55}Nd_5$ phase and its thermodynamic stability

Shuai Zhang[1)], *Qianqian Li*[2)], *Hongcan Chen*[1)], *Qun Luo*[1),✉], *and Qian Li*[1,3),✉]

1) State Key Laboratory of Advanced Special Steels, Shanghai Key Laboratory of Advanced Ferrometallurgy, School of Materials Science and Engineering, Shanghai University, Shanghai 200444, China
2) Materials Genome Institute, Shanghai University, Shanghai 200444, China
3) National Engineering Research Center for Magnesium Alloys, Chongqing University, Chongqing 400044, China
(Received: 30 August 2021; revised: 12 November 2021; accepted: 1 December 2021)

Abstract: The quasicrystal phase is beneficial to increasing the strength of magnesium alloys. However, its complicated structure and unclear phase relations impede the design of alloys with good mechanical properties. In this paper, the $Mg_{40}Zn_{55}Nd_5$ icosahedral quasicrystal (I-phase) structure is discovered in an as-cast Mg–58Zn–4Nd alloy by atomic resolution high-angle annular dark-field scanning transmission electron microscopy (HAADF-STEM). A cloud-like morphology is observed with $Mg_{41.6}Zn_{55.0}Nd_{3.4}$ composition. The selected area electronic diffraction (SAED) analysis shows that the icosahedral quasicrystal structure has 5-fold, 4-fold, 3-fold, and 2-fold symmetry zone axes. The thermodynamic stability of the icosahedral quasicrystal is investigated by differential scanning calorimetry (DSC) in the annealed alloys. When annealed above 300°C, the $Mg_{40}Zn_{55}Nd_5$ quasicrystal is found to decompose into a stable ternary phase $Mg_{35}Zn_{60}Nd_5$, a binary phase MgZn, and α-Mg, suggesting that the quasicrystal is a metastable phase in the Mg–Zn–Nd system.

Keywords: icosahedral quasicrystal; crystal structure; thermodynamic stability; Mg–Zn–Nd alloys

1. Introduction

With increasing emphasis on energy conservation and emissions reduction, Mg alloys, as one of the lightest metallic structure materials, have attracted much attention in many fields [1–9]. However, the low tensile strength and poor ductility of Mg alloys limit its applications. Methods used to improve the mechanical properties of Mg alloys include principally selecting an ideal strengthening phase [10–16] and using a suitable processing technology [17–21]. Obtaining the strengthening phase by adjusting the alloy composition is one of the most common ways. Zn exhibits a hexagonal close-packed crystal structure, which is similar to that of Mg. The addition of Zn is beneficial to the strengthening of Mg alloys. However, Mg–Zn binary alloys, whose grains are relatively coarse, have poor fluidity and are prone to defects such as shrinkage and porosity under the casting process [22]. Rare-earth (RE) elements enhance the bonding of atoms in the Mg alloy due to its unique electronic arrangement structure. Adding RE elements to the Mg–Zn alloy reduces casting defects and improves the comprehensive mechanical properties [23]. These are attributed to the solution strengthening of the RE element and the formation of intermetallic compounds such as the icosahedral quasicrystal phase (I-phase) with a unique structure. Wu *et al*. [24] found that the eutectic phase in an extruded Mg–Ce–Zn–Zr alloy is mainly composed of $Mg_{12}Ce$ and $Mg_{17}Ce_2$ compounds with the tensile strength reaching 251 MPa at room temperature. The extruded Mg–5.53Zn–1.35Y–0.42Zr containing an I-phase shows an ultimate tensile strength of about 340 MPa, which is higher than those of ZK60 extruded at the same condition (290 MPa) [25]. Zhang *et al*. [26] found that the strengthening effect of the I-phase is the most significant thing among the Mg_7Zn_3, W-phase, and I-phase in Mg–Zn–Gd. The tensile strength of the as-cast Mg–Zn–Gd alloy containing the I-phase is 173 MPa. Introducing the I-phase to AZ91, the tensile strength increased from 161 to 223 MPa, i.e., by 38% [27].

The high strength, high hardness [28], and quasiperiodic lattice structure of the quasicrystal are the reasons for the strengthening effect. The I-phase has characteristics of icosahedral symmetry with six 5-fold axes, ten 3-fold axes, and fifteen 2-fold axes, and maintains a proper coherent interface with the Mg matrix. The investigation of Bae *et al*. [29] showed that the orientation relationship between the α-Mg and the quasicrystal phase is 2-fold and 5-fold//α-Mg [30]. In addition, high-hardness quasicrystal particles can effectively impede the migration of grain boundary and dislocations.

Quasicrystals are a class of materials that exhibit a long-range order in their atomic arrangement but lack translational symmetry (periodicity). In 1984, Shechtman *et al*. [31] first found an icosahedral phase with a 5-fold rotational sym-

✉ Corresponding authors: Qun Luo E-mail: qunluo@shu.edu.cn; Qian Li E-mail: cquliqian@cqu.edu.cn

metry in a rapidly solidified Al–Mn aluminum alloy. Subsequent studies about quasicrystals mainly concentrated on Al alloys. In the late 20th and early 21st centuries, stable quasicrystal phases were reported to exist in Mg–Al–X (X = Cu, Pd, Ag, Pt) and Mg–Zn–M (M = Ga, Al, RE) systems. An icosahedral quasicrystal would be easily obtained through rapid solidification and slow cooling under normal cast conditions in Mg–Zn–RE systems. Icosahedral quasicrystals are usually divided into two categories: (1) the Al–Tm type with a structural unit of a Mackay icosahedron (quasi-lattice constant a_R = 0.46 nm) and (2) the Al_6Li_3Cu and $Mg_{32}(Al,Zn)_{49}$, which are Pauling concentric icosahedral symmetric (a_R = 0.51 nm). To date, the three-dimensional symmetry structure of the icosahedral quasicrystal is still poorly understood because of its complexity.

The formation mechanism of a quasicrystal mainly includes the peritectic reaction and direct precipitation [32–34], which may lead to different morphologies. The icosahedral quasicrystal in Mg–Zn–Nd is spherical [35] and is dispersed in the matrix. However, the quasicrystal phase is continuous and reticulated in Mg–Zn–Y/Gd alloys, which tends to form cracks under over-high stress. Therefore, the small spherical quasicrystal particle is beneficial to improving the mechanical properties. The chemical composition is also an important factor for the morphology of the quasicrystal. It was reported that when the atomic ratio of Mg/Zn is maintained around 2.5–2.6 with 1.2at% Nd, the spherical quasicrystal phase is uniformly distributed in the Mg_7Zn_3 matrix phase, and the number density of the quasicrystal phase is the largest [36]. However, Yang *et al*. [37] found that the quasicrystal existed in the Mg–45Zn–1.5Nd alloy with an Mg/Zn ratio of 3.2. In addition, the thermodynamic stability of the quasicrystal is uncertain. Huang *et al*. [38] believed that there was no quasicrystal in the equilibrium alloy, whereas Mostafa and Medraj [39] argued that the quasicrystal was an equilibrium phase. The chemical composition and existing temperature range of the quasicrystal are rarely reported, although they are highly desirable for the design of quasicrystal strengthening Mg alloys.

In this work, the stable condition and transformation process of the quasicrystal phase in the Mg–Zn–Nd system were investigated through differential scanning calorimetry (DSC) and an annealed alloy. The structure of the $Mg_{40}Zn_{55}Nd_5$ quasicrystal phase was revealed by atomic resolution high-angle annular dark-field scanning transmission electron microscopy (HAADF-STEM). The existing temperature range and phase transformation of the quasicrystal were then studied by annealing the alloys at different temperatures. Finally, phase relations of the Mg–Zn–Nd system were provided.

2. Experimental

The alloys were produced from commercially pure Mg (99.99%), pure Zn (99.99%), pure Nd (99.99%), and Mg–30Nd blocks. Four alloy ingots (~100 g each) with different chemical compositions were prepared by vacuum induction melting. The four alloy samples were cut from each ingot and labeled #1, #2, #3, and #4. The actual composition of Mg–Zn–Nd alloys was measured by Optima 7300DV inductively coupled plasma atomic emission spectrometry (ICP) with the results shown in Table 1. The alloys were then annealed at 300, 350, and 400°C at different times in muffle furnaces and were cooled by water quenching.

Table 1. Actual composition of Mg–Zn-Nd alloys wt%

Alloy number	Mg	Zn	Nd
#1	38.05	58.05	3.90
#2	41.88	46.72	11.40
#3	47.35	27.07	25.58
#4	58.76	7.06	34.18

Powder specimens of all as-cast and annealed alloys were analyzed by D2 PHASER X-ray diffraction (XRD) at a 2θ range of 10° to 75° with a scanning rate of 2°/min to identify phase constitutions. Microstructures of the alloys were studied through a JSM-7500 scanning electron microscope (SEM), and the phases' chemical compositions were determined using energy-dispersive X-ray spectroscopy (EDS). The quasicrystal structure was characterized by atomic resolution high-angle annular dark-field scanning transmission electron microscopy (HAADF-STEM) on a Themis ETEM microscope, and the wafer sample was prepared by focusing ion beam (FIB, Helios G4 UC). The phase transformation temperature of as-cast alloy #1 was measured by NETZSCH 404F3 DSC from room temperature to 500°C with a heating rate of 10°C/min under a high purity argon atmosphere with a flowing rate of 50 mL/min.

3. Results and discussion

3.1. Quasicrystal phase in as-cast Mg–Zn–Nd alloys

Fig. 1 shows the isothermal section of the Mg–Zn–Nd system at 300°C calculated by Zhang *et al*. [40]. The selected compositions of alloys #1 and #2 are situated within the controversial phase regions (marked by red dash lines) in which the icosahedral quasicrystal phase may exist. As discussed previously, Huang *et al*. [38] and Mostafa and Medraj [39] held opposite opinions on whether the I-phase was an equilibrium phase in the controversial phase regions. Alloys #3 and #4 were selected to determine whether the I-phase

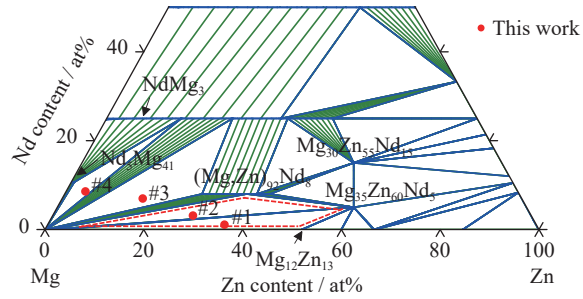

Fig. 1. Calculated local isothermal section of the Mg–Zn–Nd system at 300°C. The thermodynamic database is from the literature [40]. Regions marked by red dash lines are the controversial phase regions [38–39].

forms in the Mg-rich corner or not.

Fig. 2 shows the XRD patterns of the as-cast alloys. All phases are identified in all alloys except for alloy #1, which exhibits some unknown diffraction peaks at 36°–39° and 64°–67° (marked by stars). These unknown peaks are similar to those of the spherical I-phase in the Mg–Zn–Nd system reported by Zhang *et al*. [41]. The backscattered electron image of the as-cast alloy #1 (Fig. 3(a)) shows a dual-phase microstructure consisting of a cloud-like phase and the Mg_7Zn_3 matrix. In addition, the white strip-like phase along the crystal boundary cannot be detected by XRD because of its low content. It could be the eutectic microstructure or ternary intermetallic compound inferred from the literature [41]. The average composition of the cloud-like phase detected by EDS is approximately $Mg_{41.6}Zn_{55.0}Nd_{3.4}$, which is very close to the I-phase ($Mg_{40.54}Zn_{54.68}Nd_{4.78}$) reported by Zhang *et al*. [41]. Unknown diffraction peaks in alloy #1 are also similar to the sharp diffraction peaks determined by Niikura *et al*. [42] in a rapidly solidified Mg–Zn–Nd alloy. Unfortunately, the accurate crystal structure of this unknown phase is rarely reported; thereby, the full diffraction pattern of the icosahedral phase remains indistinct.

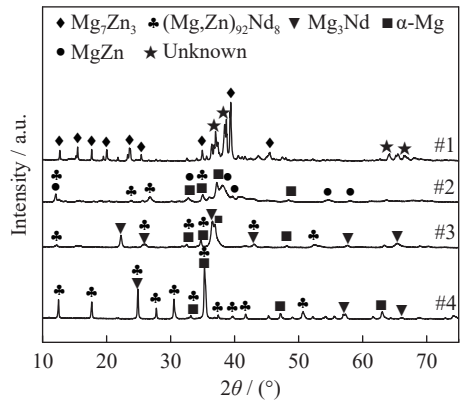

Fig. 2. XRD patterns of as-cast Mg–Zn–Nd alloys.

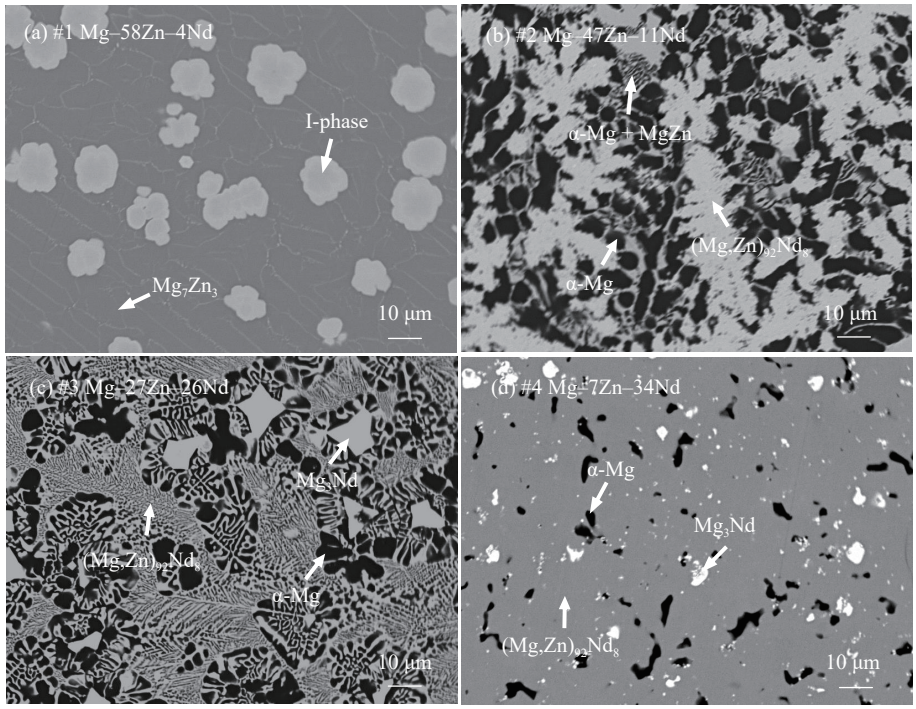

Fig. 3. Backscattered SEM images of as-cast alloys #1–#4.

Alloy #2 contains $(Mg,Zn)_{92}Nd_8$, MgZn, and α-Mg as identified from its XRD pattern in Fig. 2. However, the microstructure of alloy #2 is complex, as shown in Fig. 3(b), which consists of the primary dendritic $(Mg,Zn)_{92}Nd_8$, α-Mg, and the eutectic structure of MgZn and α-Mg. Both alloys #3 and #4 consisted of three phases of Mg_3Nd, α-Mg, and $(Mg,Zn)_{92}Nd_8$ according to their diffraction peaks. However, their microstructures are completely different. Alloy #3 has the Mg_3Nd as the primary phase, which is polygonal with sharp angles. The dark phase around the Mg_3Nd is α-Mg, and the very fine layered phase is $(Mg,Zn)_{92}Nd_8$ in Fig. 3(c). In contrast, the dendritic α-Mg shown in Fig. 3(d) is the primary phase of alloy #4. Besides, the dot-like Mg_3Nd and $(Mg,Zn)_{92}Nd_8$ form the divorced eutectic structure in the as-cast alloy #4.

It should be noted that alloys #1 and #2 may both contain the I-phase according to Fig. 1. However, the I-phase is experimentally detected only in alloy #1, which is cloud-like because it formed directly from the liquid. The formation mechanism of the I-phase is the direct precipitation in the Mg–Zn–Nd system. The composition range of I-phase formation is the phase region ($Mg_{36–100}Zn_{0–59}Nd_{0–5}$) which alloy #1 located in. Alloy #1 is selected as the main alloy for further study since the I-phase is only found in this alloy.

3.2. Quasicrystal structure of $Mg_{40}Zn_{55}Nd_5$

Fig. 4 displays the electron diffraction patterns (EDPs) of the cloud-like phase in alloy #1. Strong diffraction spots

show a 5-fold symmetry in Fig. 4(b), which is one of the unique features of the quasicrystal phase and is impossible to appear in classic crystallography. Therefore, the cloud-like phase can be rationally identified as quasicrystals. Generally, the 5-fold EDP of quasicrystals can generate pentagons in real space. The atomic structure has been further deeply studied by the HAADF-STEM image, the contrast of which is directly connected to the atomic number and chemical composition. Fig. 4(a) shows the HAADF-STEM image of the I-phase taken along the 5-fold axis. Five clear brighter dots with a separation angle of 36° correspond to the heavier constituent element of Nd columns (marked by yellow) with the edge-length of 0.8 nm for each pentagon. Additionally, one pentagonal atom cluster (marked by blue) is formed by connecting another five bright dots at the center of each large pentagon above. Its side length is ~0.3 nm. The contrast of atoms in the smaller pentagonal arrangement looks obviously weaker than those in the larger ones, indicating that the consisting atoms are mixed sites of Nd and Mg or Zn. Decagons (marked by red) with an edge length of 0.16 nm could be easily recognized in the I-phase in Fig. 4(a). These atom dots may be Mg or Zn columns due to their corresponding weak contrast. Therefore, the unit consisting of two pentagons and five decagons covers the whole plane but partially overlaps. This indicates that the quasicrystal structure is

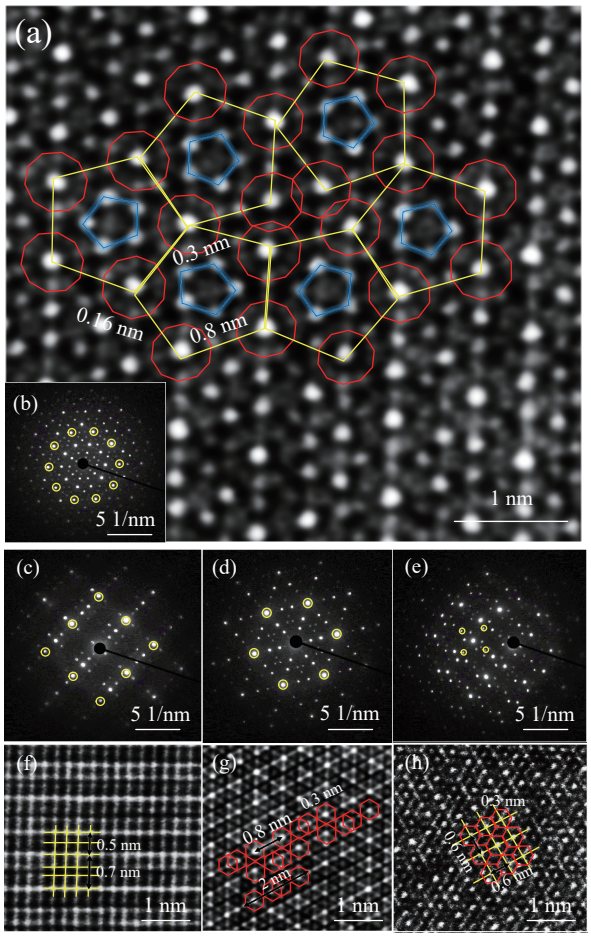

Fig. 4. SAED patterns and HAADF-STEM images of the I-phase along the 5-fold (a, b), 4-fold (c, f), 3-fold (d, g), and 2-fold (e, h) axes.

defective compared to crystals.

The 4-fold EDP and the atomic-scale image (Fig. 4(c) and (f)) of the I-phase in the Mg–Zn–Nd system were observed for the first time. In Fig. 4(f), Nd atoms are stacking in the form of a layer structure with four bright dots forming a rectangle. The distance between the brighter and larger Nd atomic layers is 0.5 or 0.7 nm. The atomic arrangement is too close to distinguish a single atom in some planes because it is beyond the resolution of the HAADF-STEM (~0.136 nm). There are several dark atom layers between two Nd atoms layers due to the intercalation of Mg atoms in these layers. Fig. 4(g) shows the atoms arranged in hexagons (marked by red) along the 3-fold symmetric axis with a side length of 0.3 nm. Four hexagons compose a group with a total width of 2 nm. The distance between the central Nd atoms of adjacent hexagons is 0.8 nm. Fig. 4(h) presents the HAADF-STEM image taken along the 2-fold zone axis. Hexagons (marked by red) with a side length of 0.3 nm consisting of Mg or Zn atoms are neatly arranged on the plane. Nd atoms in the center of each hexagon regularly arrange along a straight line with a separation distance of 0.6 nm. Atomic arrangements are quasiperiodic from four directions, further proving the construction of the $Mg_{40}Zn_{55}Nd_5$ icosahedral quasicrystal structure.

The highly symmetrical structure of the I-phase makes it a good strengthening phase. The second-phase/matrix debonding is generally considered as one of the sources of the cracks' origin during the tensile process. The I-phase has multiple symmetry axes in all directions, leading to the semi-coherent or coherent interface with the α-Mg. Bae *et al*. [29] observed that the orientation relationship is 2-fold and 5-fold//$\{10\bar{1}0\}_{\alpha\text{-Mg}}$. The atomic bonding of the I-phase/α-Mg interface is rigid enough to be retained under high stress. In addition, the hardness of the I-phase is up to HV 154 [37], and the I-phase exhibits individual cloud-like particles in the Mg–Zn–Nd system. The low strain energy interface provides a lower driving force for the growth of I-phase particles, which makes the particle size stable. The I-phase particle is hard to deform or grow at a higher temperature and prevents grain growth. The stable interface with the matrix and the high hardness of I-phase particles can effectively impede the dislocation and grain boundary to improve mechanical properties.

3.3. Thermodynamic stability of the $Mg_{40}Zn_{55}Nd_5$ quasicrystal

Fig. 5(a) shows the DSC heating curve of alloy #1, which indicates two endothermic peaks at 344.9°C and 357.4°C. To clarify the phase transitions, alloy #1 is annealed at 300, 350, and 400°C. Fig. 5(b) and (c) displays the microstructures of alloy #1 held at 350 and 400°C for 10 h, respectively. The alloy partially melts while annealing at 350°C. The microstructure after quenching is composed of the ternary phase $Mg_{35}Zn_{60}Nd_5$, binary phase Mg_7Zn_3, MgZn, and α-Mg. It is reported that the Mg_7Zn_3 melts at about 343°C [43]. Compared with phases in the as-cast alloy #1, the transformation Mg_7Zn_3 → MgZn + α-Mg may occur at 344.9°C, and the

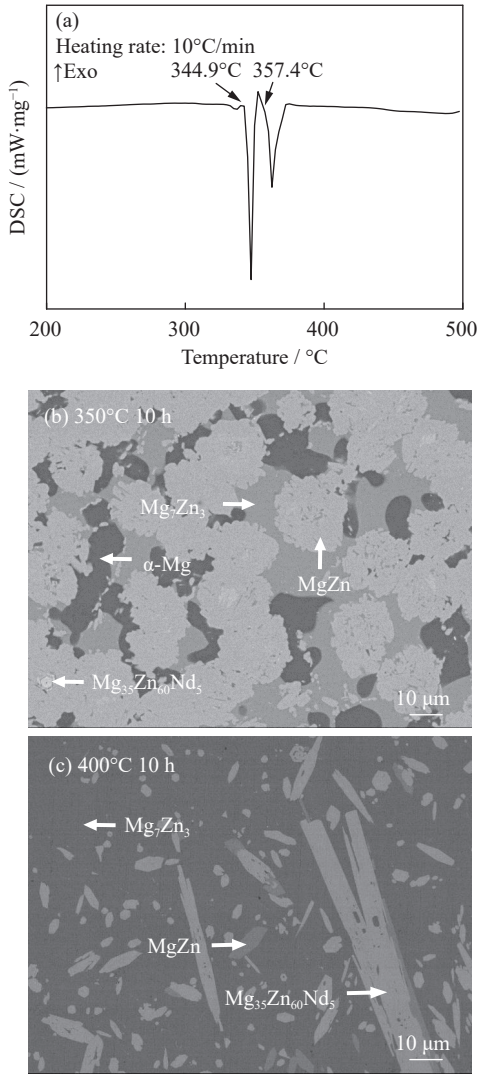

Fig. 5. (a) DSC heating curve of the as-cast alloy #1 and the microstructure of alloy #1 annealed at (b) 350°C and (c) 400°C. Exo in (a) represents exothermic.

transformation I-phase → $Mg_{35}Zn_{60}Nd_5$ + MgZn + α-Mg may begin at 357.4°C.

The microstructure of alloy #1 annealed at 400°C consists of three phases: $Mg_{35}Zn_{60}Nd_5$, MgZn, and Mg_7Zn_3. The absence of α-Mg in alloy #1 after annealing at 400°C is attributed to the complete melt. The quenching process is equivalent to the re-solidification for alloy #1. Hence, the Mg_7Zn_3 becomes the matrix instead of the α-Mg. The cooling rate of quenching from 400°C is lower than that of the casting process and thus, the rod-like ternary phase $Mg_{35}Zn_{60}Nd_5$ forms in the annealing alloy #1 (Fig. 5(c)). From Fig. 5(b) and (c), the I-phase rapidly disappears when liquid is present. Therefore, the solid-state phase transformation of the I-phase is investigated blowing at the determined melting temperature of 357.4°C.

Fig. 6 shows the microstructures of alloy #1 annealed at 300°C for 60, 110, and 170 d. Mg_7Zn_3 disappears rapidly after annealing at 300°C for 60 d, substituted by α-Mg and MgZn phases. The MgZn phase layer forms around the I-phase. After annealing at 300°C for 110 d, the thickness of the MgZn layer increases, and the size of the I-phase decreases. Holding at 300°C for 170 d, Nd atoms from the I-phase diffuse into the MgZn layer, finally forming a stable $Mg_{35}Zn_{60}Nd_5$ ternary phase with $Mg_{29.1}Zn_{63.9}Nd_{7.0}$ composition as determined by EDS. However, there is still a small amount of I-phase in the alloy. The average composition of the I-phase is about $Mg_{43.1}Zn_{53.5}Nd_{3.4}$ and $Mg_{40.3}Zn_{55.5}Nd_{4.2}$ when annealed at 300°C for 60 and 170 d. Atomic contents of the I-phase change slightly during annealing, which indicates that the I-phase transformation is very slow at 300°C. As observed from the microstructure evolution, the I-phase will decompose into $Mg_{35}Zn_{60}Nd_5$, α-Mg, and MgZn above 300°C if the holding time is long enough. This suggests that the icosahedral quasicrystal should be an unstable phase in the Mg–Zn–Nd system. Mostafa and Medraj [39] considered the quasicrystal as an equilibrium phase, which might be due to the relatively short annealing time (40 d).

Considering the formation enthalpy of the I-phase in Mg–Zn–Nd, the thermodynamic stability is compared with the I-phase in Mg–Zn–Y. Due to the metastable I-phase with a non-translational symmetry crystal structure, it is hard to calculate the formation enthalpy through first-principles calculation. The reported formation enthalpy of the I-phase in Mg–Zn–Y was calculated by the CALPHAD-type thermo-

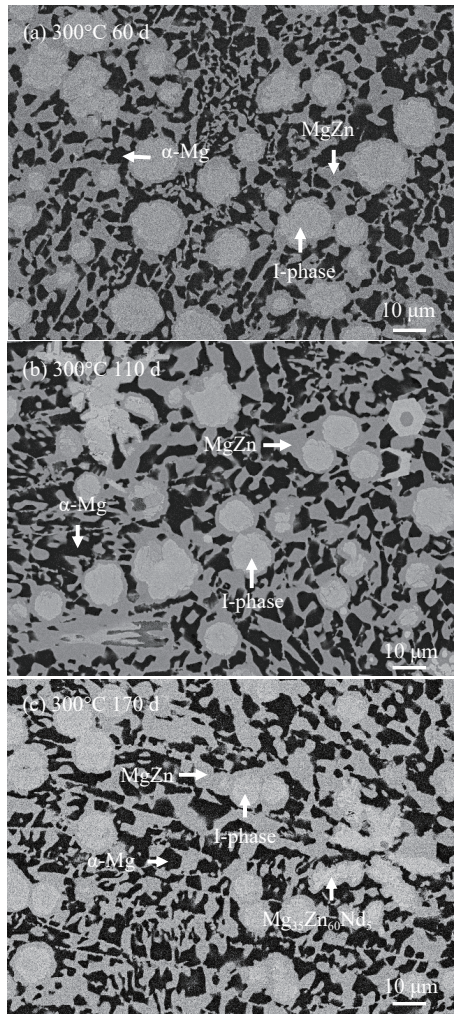

Fig. 6. Microstructure of alloy #1 annealed at 300°C for (a) 60 d, (b) 110 d, and (c) 170 d.

dynamic database [44]. However, the metastable I-phase in the Mg–Zn–Nd system was seldom reported in the thermodynamic database of Mg–Zn–Nd. Its formation enthalpy is also hard to obtain by the CALPHAD approach. Therefore, we can only refer to the lower limit of the formation enthalpy by comparing it with that of adjacent phases. The I-phase transforming into $Mg_{35}Zn_{60}Nd_5$ and α-Mg is observed in the annealing experiment. According to the endothermic reaction (Eq. (1)), the formation enthalpy ΔH_f of the I-phase is obtained by Eq. (2). Formation enthalpies of pure Mg, $Mg_{35}Zn_{60}Nd_5$, and $Mg_{47}Zn_{45}Nd_8$ are calculated as shown in Table 2. It can be inferred that the $\Delta H_f(Mg_{40}Zn_{55}Nd_5) > -20.8$ kJ·mol^{-1}·atom^{-1}.

$$10.2\text{I-phase}(Mg_{40}Zn_{55}Nd_5) = 8.6Mg_{35}Zn_{60}Nd_5 + 60Mg + Mg_{47}Zn_{45}Nd_8 \quad (1)$$

$$10.2\Delta H_f(Mg_{40}Zn_{55}Nd_5) - 8.6\Delta H_f(Mg_{35}Zn_{60}Nd_5) - 60\Delta H_f(Mg) - \Delta H_f(Mg_{47}Zn_{45}Nd_8) > 0 \quad (2)$$

Table 2. Calculated formation enthalpies of phases in Mg–Zn–Nd/Y at 25°C

Alloy	Phase	Formation enthalpy / (kJ·mol^{-1}·atom^{-1})
Mg–Zn–Nd [This work]	Mg	0
	$Mg_{35}Zn_{60}Nd_5$	–21.9
	$Mg_{47}Zn_{45}Nd_8$*	–24.3
	I-phase ($Mg_{40}Zn_{55}Nd_5$)	>–20.8
Mg–Zn–Y [44]	I-phase ($Mg_{30}Zn_{60}Y_{10}$)	–28.5
	$Mg_{28}Zn_{65}Y_7$	–27.7
	$Mg_{25}Zn_{50}Y_{25}$	–41.9
	$Mg_{22}Zn_{62}Y_{16}$	–27.4

Note: *$Mg_{47}Zn_{45}Nd_8$ is a special case of $(Mg,Zn)_{92}Nd_8$.

The formation enthalpy of the I-phase ($Mg_{30}Zn_{60}Y_{10}$) is –28.5 kJ·mol^{-1}·atom^{-1} [44]. Therefore, the thermostability of the I-phase in the Mg–Zn–Nd system is less stable than that in Mg–Zn–Y. Table 2 also lists the formation enthalpies of other ternary phases. In all ternary phases, the I-phase is more prone to transform, whether in the Mg–Zn–Nd system or the Mg–Zn–Y system.

Fig. 7(a) and (b) shows the liquid projection and isothermal section at 400°C of the Mg–Zn–Nd system, revealing the primary $Mg_{35}Zn_{60}Nd_5$ phase formed by the liquid phase in the phase regions of alloys #1 and #2 (marked by yellow dash lines in Fig.7(a)). However, the fast solidification process prevents the complete diffusion of atoms, implying that the I-phase replacing the $Mg_{35}Zn_{60}Nd_5$ forms first in the as-cast alloy #1.

Alloys #2–#4 are also annealed at 400°C. Alloy #2 deforms due to the presence of liquid when it is held at 400°C for 19 d. Fig. 7(b) shows the isothermal section of the Mg–Zn–Nd system and the determined phase compositions of the alloys at 400°C. XRD patterns in Fig. 7(c) show that the annealed alloy #2 contains $Mg_{35}Zn_{60}Nd_5$, MgZn, and α-Mg. Both annealed alloys #3 and #4 contain $(Mg, Zn)_{92}Nd_8$, Mg_3Nd, and α-Mg. Phase constitutions of annealed alloys #2 and #3 coincide with the calculated isothermal section at

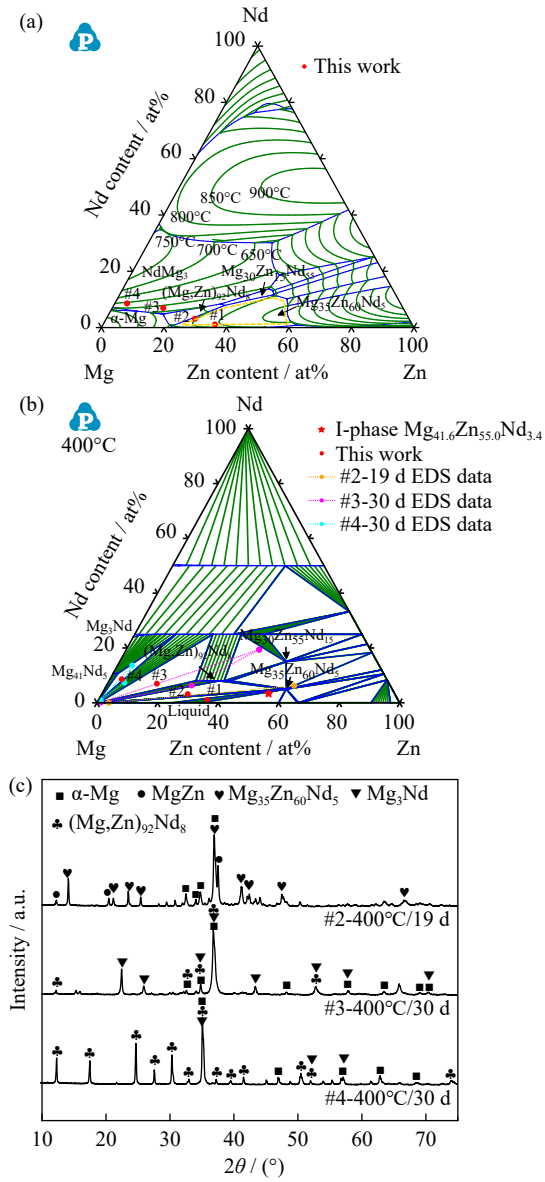

Fig. 7. (a) Liquid projection and (b) isothermal section at 400°C of the Mg–Zn–Nd system and (c) XRD patterns of annealed alloys #2–#4.

400°C, and the I-phase is not found, while the solid solution of Zn in Mg_3Nd for alloy #3 is much larger than the calculated result. Moreover, $(Mg, Zn)_{92}Nd_8$ of alloy #4 is not in the calculated phase region.

In short, the I-phase forms directly by the liquid when the alloy composition is in the phase region of alloy #1. The I-phase gradually decomposes into equilibrium phases while annealing above 300°C. The transformation rate increases with the increase of temperature and the appearance of the liquid phase.

4. Conclusions

The morphology and atomic structure of the icosahedral quasicrystal phase in the Mg–Zn–Nd system are investigated by ultrahigh-resolution HAADF-STEM. In addition, the thermodynamic stability of quasicrystal is studied, and the formation and transformation conditions are given. The fol-

lowing conclusions are drawn.

(1) The quasicrystal can form by conventional casting conditions. The quasicrystal is cloud-like with the composition of $Mg_{41.6}Zn_{55.0}Nd_{3.4}$ in the as-cast alloy. The alloy composition range required for quasicrystal formation is the phase region ($Mg_{36–100}Zn_{0–59}Nd_{0–5}$) which alloy #1 located in.

(2) The quasicrystal shows an icosahedral structure with 5-fold, 4-fold, 3-fold, and 2-fold symmetry in the Mg–Zn–Nd system. Two-dimensional atomic arrangements viewed from four directions are fully displayed. Nd atoms form different pentagons with side lengths of 0.3 and 0.8 nm along the 5-fold axis, whereas Nd atoms are arranged in a straight line when viewed from the other three axes. The Mg or Zn atoms surrounding them form hexagons with a side length of 0.3 nm along the 3-fold and 2-fold axes.

(3) The $Mg_{40}Zn_{55}Nd_5$ icosahedral quasicrystal is a metastable phase of which the formation enthalpy is higher than –20.8 $kJ·mol^{-1}·atom^{-1}$. It decomposes into $Mg_{35}Zn_{60}Nd_5$, MgZn, and α-Mg above 300°C. The increase of temperature and the presence of liquid facilitate the decomposition of the quasicrystal. The quasicrystal exists when annealed at 300°C for 170 d, but it completely dissolves when liquid appears when annealed at 350°C for 10 h.

Acknowledgements

This work was financially supported by the National Natural Science Foundation of China (Nos. 51871143 and 11972219), the Science and Technology Committee of Shanghai (No. 19010500400), Shanghai Rising-Star Program (No. 21QA1403200), and the Independent Research Project of State Key Laboratory of Mechanical Transmissions of China (No. SKLMT-ZZKT-2021M11).

Conflict of Interest

The authors declare no conflict of interest.

References

[1] Y.Z. Ma, C.L. Yang, Y.J. Liu, F.S. Yuan, S.S. Liang, H.X. Li, and J.S. Zhang, Microstructure, mechanical, and corrosion properties of extruded low-alloyed Mg–*x*Zn–0.2Ca alloys, *Int. J. Miner. Metall. Mater.*, 26(2019), No. 10, p. 1274.

[2] N.A. Ali and M. Ismail, Advanced hydrogen storage of the Mg–Na–Al system: A review, *J. Magnes. Alloys*, 9(2021), No. 4, p. 1111.

[3] Q. Li, X. Lin, Q. Luo, Y.A. Chen, J.F. Wang, B. Jiang, and F.S. Pan, Kinetics of the hydrogen absorption and desorption processes of hydrogen storage alloys: A review, *Int. J. Miner. Metall. Mater.*, 29(2022), No. 1, p. 32.

[4] Y. Li, Y. Jiang, B. Liu, Q. Luo, B. Hu, and Q. Li, Understanding grain refining and anti Si-poisoning effect in Al–10Si/Al–5Nb–B system, *J. Mater. Sci. Technol.*, 65(2021), p. 190.

[5] J.L. Su, J. Teng, Z.L. Xu, and Y. Li, Biodegradable magnesium-matrix composites: A review, *Int. J. Miner. Metall. Mater.*, 27(2020), No. 6, p. 724.

[6] H. Elkholy, H. Othman, I. Hager, M. Ibrahim, and D. de Ligny, Thermal and optical properties of binary magnesium tellurite glasses and their link to the glass structure, *J. Alloys Compd.*, 823(2020), art. No. 153781.

[7] J.F. Song, J. She, D.L. Chen, and F.S. Pan, Latest research advances on magnesium and magnesium alloys worldwide, *J. Magnes. Alloys*, 8(2020), No. 1, p. 1.

[8] Y.C. Zhou, Q. Luo, B. Jiang, Q. Li, and F.S. Pan, Strength-ductility synergy in $Mg_{98.3}Y_{1.3}Ni_{0.4}$ alloy processed by high temperature homogenization and rolling, *Scripta Mater.*, 208(2022), art. No. 114345.

[9] W.Q. Tang, J.Y. Lee, H.M. Wang, D. Steglich, D.Y. Li, Y.H. Peng, and P.D. Wu, Unloading behaviors of the rare-earth magnesium alloy ZE10 sheet, *J. Magnes. Alloys*, 9(2021), No. 3, p. 927.

[10] T.C. Xie, H. Shi, H.B. Wang, Q. Luo, Q. Li, and K.C. Chou, Thermodynamic prediction of thermal diffusivity and thermal conductivity in Mg–Zn–La/Ce system, *J. Mater. Sci. Technol.*, 97(2022), p. 147.

[11] M. Gao, Z. Ma, I.P. Etim, L.L. Tan, and K. Yang, Microstructure, mechanical and corrosion properties of Mg–Zn–Nd alloy with different accumulative area reduction after room-temperature drawing, *Rare Met.*, 40(2021), No. 4, p. 897.

[12] H.J. Si, Y.X. Jiang, Y. Tang, and L.J. Zhang, Stable and metastable phase equilibria in binary Mg–Gd system: A comprehensive understanding aided by CALPHAD modeling, *J. Magnes. Alloys*, 7(2019), No. 3, p. 501.

[13] Y.L. Guo, B. Liu, W. Xie, Q. Luo, and Q. Li, Anti-phase boundary energy of β series precipitates in Mg–Y–Nd system, *Scripta Mater.*, 193(2021), p. 127.

[14] L. Li, D.J. Li, X.Q. Zeng, A.A. Luo, B. Hu, A.K. Sachdev, L.L. Gu, and W.J. Ding, Microstructural evolution of Mg–Al–Re alloy reinforced with alumina fibers, *J. Magnes. Alloys*, 8(2020), No. 3, p. 565.

[15] H. Zengin and Y. Turen, Effect of Y addition on microstructure and corrosion behavior of extruded Mg–Zn–Nd–Zr alloy, *J. Magnes. Alloys*, 8(2020), No. 3, p. 640.

[16] Q. Li, X.D. Peng, and F.S. Pan, Magnesium-based materials for energy conversion and storage, *J. Magnes. Alloys*, 9(2021), No. 6, p. 2223.

[17] Z. Zhang, J.H. Zhang, J. Wang, Z.H. Li, J.S. Xie, S.J. Liu, K. Guan, and R.Z. Wu, Toward the development of Mg alloys with simultaneously improved strength and ductility by refining grain size via the deformation process, *Int. J. Miner. Metall. Mater.*, 28(2021), No. 1, p. 30.

[18] Y.B. Wang, S.S. Jia, M.G. Wei, L.M. Peng, Y.J. Wu, and X.T. Liu, Research progress on solidification structure of alloys by synchrotron X-ray radiography: A review, *J. Magnes. Alloys*, 8(2020), No. 2, p. 396.

[19] Q. Li, Y.F. Lu, Q. Luo, X.H. Yang, Y. Yang, J. Tan, Z.H. Dong, J. Dang, J.B. Li, Y. Chen, B. Jiang, S.H. Sun, and F.S. Pan, Thermodynamics and kinetics of hydriding and dehydriding reactions in Mg-based hydrogen storage materials, *J. Magnes. Alloys*, 9(2021), No. 6, p. 1922.

[20] Y.P. Pang, D.K. Sun, Q.F. Gu, K.C. Chou, X.L. Wang, and Q. Li, Comprehensive determination of kinetic parameters in solid-state phase transitions: An extended jonhson–mehl–avrami–kolomogorov model with analytical solutions, *Cryst. Growth Des.*, 16(2016), No. 4, p. 2404.

[21] F. Samadpour, G. Faraji, and A. Siahsarani, Processing of AM60 magnesium alloy by hydrostatic cyclic expansion extrusion at elevated temperature as a new severe plastic deformation method, *Int. J. Miner. Metall. Mater.*, 27(2020), No. 5, p. 669.

[22] X. Gao and J.F. Nie, Structure and thermal stability of primary intermetallic particles in an Mg–Zn casting alloy, *Scripta Mater.*, 57(2007), No. 7, p. 655.

[23] Q. Luo, Y.L. Guo, B. Liu, Y.J. Feng, J.Y. Zhang, Q. Li, and

K.C. Chou, Thermodynamics and kinetics of phase transformation in rare earth-magnesium alloys: A critical review, *J. Mater. Sci. Technol.*, 44(2020), p. 171.

[24] A.R. Wu, Y. Gu, and C.Q. Xia, Study of microstructure and properties of Mg–RE(Ce Nd Y)–Zn–Zr alloys, *Hot Working Technol.*, 33(2004), No. 12, p. 21.

[25] Y. Zhang, X.Q. Zeng, L.F. Liu, C. Lu, H.T. Zhou, Q. Li, and Y.P. Zhu, Effects of yttrium on microstructure and mechanical properties of hot-extruded Mg–Zn–Y–Zr alloys, *Mater. Sci. Eng. A*, 373(2004), No. 1-2, p. 320.

[26] X.P. Zhang, G.Y. Yuan, Y. Liu, and W.J. Ding, Effects of alloying elements on the microstructure and mechanical properties of Mg–Zn–Gd alloys, *Special Cast. Nonferrous Alloys*, 28(2008), No. 11, p. 882.

[27] Y.G. Jung, W. Yang, J.I. Hyun, S.K. Kim, H. Lim, and D.H. Kim, Effects of I- and W-phases under identical conditions on microstructure and mechanical properties of as-cast Mg–Zn–Y alloys at room and elevated temperatures, *Met. Mater. Int.*, 27(2021), No. 12, p. 5154.

[28] W.B. Luo, Z.Y. Xue, and W.M. Mao, Effect of heat treatment on the microstructure and micromechanical properties of the rapidly solidified $Mg_{61.7}Zn_{34}Gd_{4.3}$ alloy containing icosahedral phase, *Int. J. Miner. Metall. Mater.*, 26(2019), No. 7, p. 869.

[29] D.H. Bae, S.H. Kim, D.H. Kim, and W.T. Kim, Deformation behavior of Mg–Zn–Y alloys reinforced by icosahedral quasicrystalline particles, *Acta Mater.*, 50(2002), No. 9, p. 2343.

[30] S.M. Zhu, T.B. Abbott, M.A. Gibson, J.F. Nie, and M.A. Easton, The influence of minor Mn additions on creep resistance of die-cast Mg–Al–RE alloys, *Mater. Sci. Eng. A*, 682(2017), p. 535.

[31] D. Shechtman, I. Blech, D. Gratias, and J.W. Cahn, Metallic phase with long-range orientational order and no translational symmetry, *Phys. Rev. Lett.*, 53(1984), No. 20, p. 1951.

[32] A. Langsdorf, F. Ritter, and W. Assmus, Determination of the primary solidification area of the icosahedral phase in the ternary phase diagram of Zn–Mg–Y, *Philos. Mag. Lett.*, 75(1997), No. 6, p. 381.

[33] E. Abe, T.J. Sato, and A.P. Tsai, Structure and phase transformation of the Zn–Mg-rare-earth quasicrystals, *Mater. Sci. Eng. A*, 294-296(2000), p. 29.

[34] S. Yi, E.S. Park, J.B. Ok, W.T. Kim, and D.H. Kim, (Icosahedral phase+α-Mg) two phase microstructures in the Mg–Zn–Y ternary system, *Mater. Sci. Eng. A*, 300(2001), No. 1-2, p. 312.

[35] J.S. Zhang, J. Yan, W. Liang, C.X. Xu, and C.L. Zhou, Icosahedral quasicrystal phase in Mg–Zn–Nd ternary system, *Mater. Lett.*, 62(2008), No. 30, p. 4489.

[36] C.P. Yang, *Effect of Solidification Rate and Heattreatment on Microstructure Evolution of Mg–Zn–Nd Quasicrystal Alloy* [Dissertation]. University of Jinan, Jinan, 2015, p. 40.

[37] L. Yang, H. Hou, Y.H. Zhao, X.M. Yang, and X.J. Hao, Effects of heat treatment on microstructure and properties of Mg–45Zn–1.5Nd alloy, *Trans. Mater. Heat Treat.*, 35(2014), No. 8, p. 53.

[38] M.L. Huang, J.Y. Yang, H.X. Li, Y.P. Ren, H. Ding, and S.M. Hao, Research on the local equilibria in the Mg-rich coener of the Mg–Zn–Nd system at 300°C, *J. Mater. Metal.*, 7(2008), No. 2, p. 126.

[39] A. Mostafa and M. Medraj, Experimental investigation of the Mg–Nd–Zn isothermal section at 300°C, *Metals*, 5(2015), No. 1, p. 84.

[40] C. Zhang, A.A. Luo, L.M. Peng, D.S. Stone, and Y.A. Chang, Thermodynamic modeling and experimental investigation of the magnesium–neodymium–zinc alloys, *Intermetallics*, 19(2011), No. 11, p. 1720.

[41] J.S. Zhang, J. Yan, W. Liang, E.L. Du, and C.X. Xu, Microstructures of Mg–Zn–Nd alloy including small quasicrystalline grains, *J. Non Cryst. Solids*, 355(2009), No. 14-15, p. 836.

[42] A. Niikura, A.P. Tsai, A. Inoue, and T. Masumoto, New class of amorphous and icosahedral phases in Zn–Mg–rare-earth metal alloys, *Jpn. J. Appl. Phys.*, 33(1994), p. L1538.

[43] X.J. Ge, *Study on the Formation and Stability of Quasicrystal Phase in Mg–Zn–Nd Alloys* [Dissertation]. University of Jinan, Jinan, 2018, p. 39.

[44] J. Gröbner, A. Kozlov, X.Y. Fang, J. Geng, J.F. Nie, and R. Schmid-Fetzer, Phase equilibria and transformations in ternary Mg-rich Mg–Y–Zn alloys, *Acta Mater.*, 60(2012), No. 17, p. 5948.